Article

Sisyphus effects in hydrogen electrochemistry on metal silicides enabled by silicene subunit edge

Zechao Zhuang [a,1], Yong Li [b,1], Jiazhao Huang [a,1], Zilan Li [a], Kangning Zhao [a], Yunlong Zhao [d], Lin Xu [a], Liang Zhou [a], Lyudmila V. Moskaleva [b,c,*], Liqiang Mai [a,*]

[a] *State Key Laboratory of Advanced Technology for Materials Synthesis and Processing, International School of Materials Science and Engineering, Wuhan University of Technology, Wuhan 430070, China*
[b] *Institute of Applied and Physical Chemistry and Center for Environmental Research and Sustainable Technology, University of Bremen, Bremen 28359, Germany*
[c] *Department of Chemistry, University of the Free State, Bloemfontein 9300, South Africa*
[d] *Advanced Technology Institute, University of Surrey, Guildford, Surrey GU2 7XH, UK*

ARTICLE INFO

ABSTRACT

Nonmetal elements strictly govern the electrochemical performance of molybdenum compounds. Yet, the exact role played by nonmetals during electrocatalysis remains largely obscure. With intermetallic $MoSi_2$ comprising silicene subunits, we present an unprecedented hydrogen evolution reaction (HER) behavior in aqueous alkaline solution. Under continuous operation, the HER activity of $MoSi_2$ shows a more than one order of magnitude improvement in current density from 1.1 to 21.5 mA cm^{-2} at 0.4 V overpotential. Meanwhile, this activation behavior is highly reversible, such that voltage withdrawal leads to catalyst inactivation but another operation causes reactivation. Thus, the system shows dynamics strikingly analogous to the legendary *Sisyphus*' labor, which drops and recovers in a stepwise manner repeatedly, but never succeeds in reaching the top of the mountain. Isomorphic WSi_2 behaves almost the same as $MoSi_2$, whereas other metal silicides with silicyne subunits, including $CrSi_2$ and $TaSi_2$, do not exhibit any anomalous behavior. A thin amorphous shell of $MoSi_2$ is observed after reaction, within which the Si remains partially oxidized while the oxidation state of Mo is basically unchanged. First-principles calculations further reveal that the adsorption of hydroxide ions on silicene subunit edges and the subsequent Si vacancy formation in $MoSi_2$ jointly lead to the anomalous HER kinetics of the adjacent Mo active centers. This work demonstrates that the role of nonmetal varies dramatically with the electronic and crystallographic structures of silicides and that silicene structural subunit may serve as a promoter for boosting HER in alkaline media.

© 2019 Science China Press. Published by Elsevier B.V. and Science China Press. All rights reserved.

1. Introduction

The pursuit of clean energy carriers is of great significance for simultaneously addressing the global energy shortage and environmental concerns [1]. Hydrogen is an alternative fuel for its near-zero emissions and wide availability, thus developing scalable techniques for hydrogen production attracts tremendous interest [2]. Electrolytic water splitting powered by sustainable energy sources as a promising solution is burgeoning over the past decade, wherefore an efficient and low-cost catalyst for cathodic hydrogen evolution reaction (HER) is highly demanded [3,4]. Molybdenum-based catalysts that possess "Pt-like" proton adsorption and robust

conductivity, including MoS_2, Mo_2C, MoO_2, MoP, Mo_2N, MoB, and so on, have recently emerged as one of the most intriguing noble metal-free choices [5–11]. Hinging upon the selected nonmetals, Mo can accommodate different stoichiometric ratios of nonmetals with specific ion radius and electronegativity, forming various compounds that exhibit rich surface chemistry and transport behavior [12–15]. Different degrees of interatomic charge transfer in the metal–nonmetal bonds strongly affect the valence states and coordination of active Mo centers, which directly governs the HER kinetics [3,4,16]. While many Mo-based binary compounds have hitherto been chosen as candidates for catalyzing HER, few works focusing on the fate and effects of nonmetals during catalysis are demonstrated. Some nonmetals display amphoteric nature and possibly react with acid or alkaline electrolytes, complicating HER process [17–19]. The dissolution or oxidation of nonmetals can greatly further alter the surface state of catalyst, leading to an unusual proton adsorption and evolution on Mo [4,18,19]. Yet,

such uncertainties still need to be unraveled and, along-side HER activity, the surface chemistry involved on Mo-based catalysts is another vital issue.

Herein, we present for the first time an unprecedented anomalous HER behavior on an intermetallic MoSi$_2$ in alkaline media. Intermetallic MoSi$_2$ has a tetragonal $C11_b$-type structure with $I4/mmm$ space group, where Mo and Si atoms with similar electronegativity ($\chi_{Mo} = 2.16$ and $\chi_{Si} = 1.90$) align along the [0 0 1] crystallographic direction following the sequence of {Mo}, {Si′}, {Si}, {Mo′}, {Si}, {Si′} atomic layers (Fig. 1a). In particular, the Si atoms are tetragonally bonded into an unusual silicene structure that inserts into the metallic Mo layers (Fig. 1b and c). Based on these unique features, MoSi$_2$ exhibits a semimetallic nature with a narrow pseudogap and high covalent character of Mo–Si bonds due to strong orbital overlap of Mo 4d and Si 3p [20]. When MoSi$_2$ functions as an alkaline HER catalyst, one order of magnitude enhancement of catalytic activity can be achieved after a continuous operation, yielding an increased current density from 1.1 to 21.5 mA cm^{-2} at an overpotential of 0.4 V. However, the withdrawal of electrolytic voltage inactivates the MoSi$_2$ suddenly. This activation/inactivation behavior is cyclable in a repetitive way, quite analogous to the legendary *Sisyphus*' labor, which drops and recovers in a stepwise manner repeatedly, but never succeeds in attempts to reach the top of the mountain. Isomorphic WSi$_2$ behaves almost the same as MoSi$_2$, whereas other metal silicides with silicyne subunits, including CrSi$_2$ and TaSi$_2$, do not exhibit any anomalous behavior. Such phenomena can be explained experimentally and theoretically as the synergy between hydrogen evolution on Mo and silicene subunit oxidation.

2. Materials and methods

2.1. Chemicals

MoSi$_2$ (99.9%), WSi$_2$ (~325 mesh, 99.5%), CrSi$_2$ (99.9%), TaSi$_2$ (99.9%), and FeSi (99.9%) powders were purchased from Aladdin Industrial Inc. (Shanghai, China), and stored in an argon-filled glove box. Potassium hydroxide (KOH, 95%) was also purchased from Aladdin Industrial Inc. All the chemicals were used without further purification. Deionized water was used throughout the whole experiment.

2.2. Characterization

Phase identification was performed by a Bruker AXS D8 Advance powder X-ray diffractometer (Bruker, Germany) using Cu Kα radiation ($\lambda = 1.5418$ Å), in a 2θ angular range of 20°–80° with a velocity of 0.02° in 4 s. Geometric morphology was divulged by JEOL JSM-7100F scanning electron microscope (JEOL, Japan). To determine the surface states of MoSi$_2$ before and after HER, X-ray photoelectron spectroscopy was performed on an ESCALAB 250 Xi spectrometer (VG Scientific Co., UK) with an Al Kα X-ray radiation (1,486.6 eV) for excitation. A JEM-2100F field emission TEM
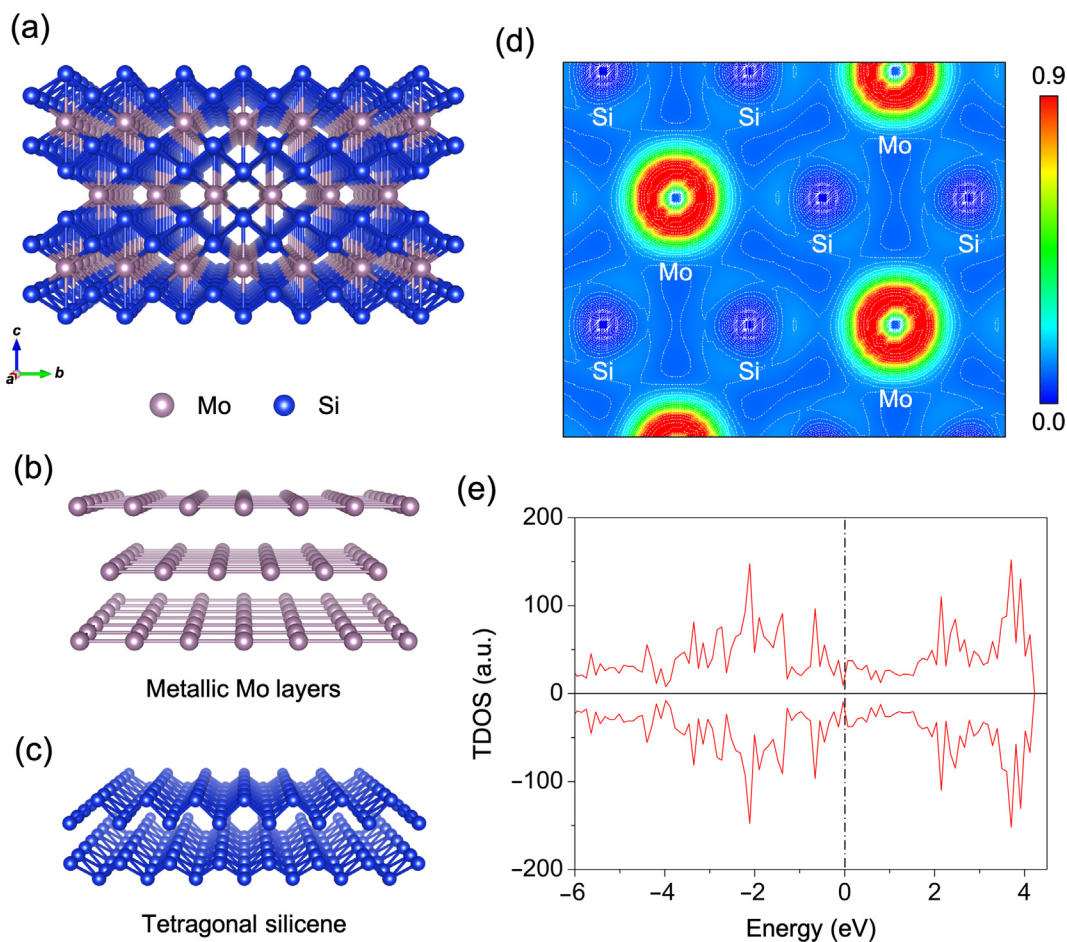
Fig. 1. (Color online) Crystal and electronic structures of MoSi$_2$. (a) Crystal structure of MoSi$_2$. Subunit structure of (b) metallic Mo layers and (c) tetragonal silicene in MoSi$_2$. (d) Electron density map on MoSi$_2$ (1 1 0) surface. (e) Calculated total density of states (TDOS) plots of MoSi$_2$. The positive and the negative parts of each DOS correspond to the spin-up and the spin-down states, respectively.

(JEOL, Japan) working at 200 kV was utilized to acquire TEM and HRTEM images in a scanning TEM mode.

2.3. Electrochemical measurements

All HER measurements were performed on a CHI 760D electro-chemical workstation (Chenhua, China), using a five-necked glass cell containing rotating disk working electrode, saturated calomel reference (SCE) electrode, and graphite rod counter electrode (Pine Instrument Co., USA). The electrodes were prepared by drop-casting the catalyst inks onto a polished glassy carbon electrode (0.196 cm^2). The electrode surface was finally loaded with HER catalyst of $0.25 \text{ mg}_{cat} \text{ cm}_{disk}^{-2}$ and a mass ratio of 5:5:1 of catalyst to carbon Vulcan XC72R to Nafion. The as-prepared electrodes were tested in 1 mol L^{-1} KOH or 0.5 mol L^{-1} H_2SO_4 solution for all electrochemical measurements. Cyclic voltammograms were recorded with a scan rate of 10 mV s^{-1} under electrode rotation rates of 1,600 r min^{-1} for gas diffusion, and then replotted as overpotential (η) versus log current (log j) to obtain Tafel plots. All the potentials were calibrated to a reversible hydrogen electrode (RHE).

2.4. DFT computations

A periodic slab model of the $MoSi_2$ (1 1 0)–p(2 × 3) surface consisting of a 16 Å × 14 Å slab (5 atomic layers) and a 20 Å vacuum layer was used to compute the electronic structure and electro-chemical mechanism of HER at the atomic and molecular level. The bottom two layers were frozen while the remaining atoms were allowed to relax without constraint. All calculations were carried out using density functional approximation as implemented in the CP2K package [21]. The generalized-gradient approximation (GGA), as parameterized by Perdew, Burke, and Ernzerhof [22,23] was utilized to compute the exchange-correlation energy. Dispersion interactions were considered in calculations by using empirical correction scheme developed by Grimme (D3) [24]. The elemental valence electrons were described using hybrid Gaussian and plane-wave basis sets, and the cutoff energy of 500 Rydberg of auxiliary plane-wave basis sets was adopted. We employed special double-ζ valence plus polarization basis sets optimized to minimize the basis set superposition errors. Core electrons were described with the norm-conserving and separable Goedecker–Teter–Hutter pseudopotentials [25]. Brillouin zone integration was performed in reciprocal space, with the k-space sampling at the gamma point only. All free energies were computed with the consideration of zero-point energy (ZPE) and enthalpy (S) at standard conditions.

3. Results and discussion

3.1. Crystal and electronic structure of $MoSi_2$

Polycrystalline $MoSi_2$ powders were purchased from commercial sources, and the crystallographic phase was confirmed by powder X-ray diffraction (XRD) analysis, as shown in Fig. S1 (online). The XRD pattern reveals that the bulk powders are mainly in the tetragonal $MoSi_2$ form with a small quantity of impurity Mo_5Si_3. Our DFT calculations indicate that the Mo sites of Mo_5Si_3 possess high proton adsorption energies (above 2 eV) and show poor HER activities. Further quantitative phase analysis of XRD data, through a reference intensity ratio method [26] indicates that this sample contains ~95% by weight of tetragonal $MoSi_2$ phase (Table S1 online). According to scanning electron microscopy (SEM) images, these powders have an irregular particle shape with a wide size distribution of 1–5 μm (Fig. S2 online). As shown in Fig. 1d, the local electron densities between neighboring Mo/Si

atoms are much higher than those in extra-nuclear regions of Si atoms. Quantitative data further show that one Mo atom gains extra 0.04 electrons from Si. This indicates that the chemical bond strength of Mo–Si increases by electron polarization from Si to Mo. The calculated total density of states (TDOS) demonstrates that $MoSi_2$ intrinsically exhibits a semimetallic behavior with conduction electrons crossing the Fermi energy (Fig. 1e). Thus, it is evident that there indeed exists an obvious covalent interaction in Mo–Si bonds. In addition, the key roles of silicene subunits in $MoSi_2$ in the electronic and transport properties of Mo atoms are confirmed.

3.2. Electrochemical behavior

An electrochemical activation behavior was firstly recorded through repeating cyclic voltammetry (CV) in 1 mol L^{-1} KOH solution. Anomalously, the cathodic current of $MoSi_2$ catalyst increases dramatically along cycling numbers, and this catalyst undergoes ~30 repeated cycles to achieve a stable and constant CV (Fig. 2a). More than an order of magnitude enhancement of catalytic current was observed after this activation, yielding an increased current density from 1.1 to 21.5 mA cm^{-2} at an overpotential of 0.4 V. This anomalous activation behavior differs significantly from those of other Mo-based catalysts, which need only several CV scans to reach an equilibrium state [11,27,28]. Also, Tafel slopes for different cycle numbers were calculated in Fig. 2b. Clearly, $MoSi_2$ catalyst after activation exhibits a much higher activity with a Tafel of 125 mV dec^{-1} than its initial state (204 mV dec^{-1}). It signifies that the rate-determining water dissociation process in alkaline media is greatly facilitated by activation. Accordingly, more sophisticated chemistry reactions should occur on the $MoSi_2$ surface, not limited to a two-electron proton reduction. This activation behavior also displays reversibility and cyclability. When one withdraws the cathodic voltage and restarts another cycling test, this $MoSi_2$ catalyst is immediately inactivated and its activity returns to the initial level (Fig. S3 online). Paralleling the first test, the catalytic current also increases continually and arrives at a maximum, as cycling proceeds, exhibiting a repeating pattern quite analogous to the legendary Sisyphus' labor. To better describe this reversible activation behavior, we further conducted chronoamperometric current-time (i-t) measurements under a fixed overpotential of 0.4 V, as shown in Fig. 2c. The first chronoamperometric curve shows an increase of one order of magnitude over 2,000 s of continuous operation, in good agreement with CV tests. The shape of subsequent curve closely matches the first one. Moreover, its current density is slightly higher, indicating a moderate enhancement in HER activity. We also obtained the i-t curves of $MoSi_2$ at −0.6 and −0.7 V (Fig. S4 online), which exhibit much higher current density than that for −0.4 V, and found the anomalous HER behavior of $MoSi_2$ under more negative cathodic potentials, where the continuous operation greatly enhances the HER activity of $MoSi_2$, which yields increased current densities from 7.29 to 34.9 mA cm^{-2} and 25.2 to 61.6 mA cm^{-2} at an overpotential of −0.6 and −0.7 V, respectively, and voltage withdrawal leads to catalyst inactivation but another operation causes reactivation. We employed ball-milling method to downsize $MoSi_2$ particles and then recorded their CV curves (Fig. S5 online). Obviously, the activation duration is similar to that of pristine $MoSi_2$ and downsizing does not accelerate the activation process. In addition, we obtained the electrochemically active surface areas (ECSAs) of $MoSi_2$ catalyst during the activation process (Fig. S6 online). After the calculation, we found that the ECSAs of $MoSi_2$ under 0, 1,000, and 2,000 s activation are 5.7, 5.6, and 5.7 mF cm^{-2}, respectively. Such a negligible change of ECSAs clearly indicates that the number density of surface active sites for $MoSi_2$ does not increase after the activation. Thus, these electrochemical results further confirm that the

(a)

(b)

(c)
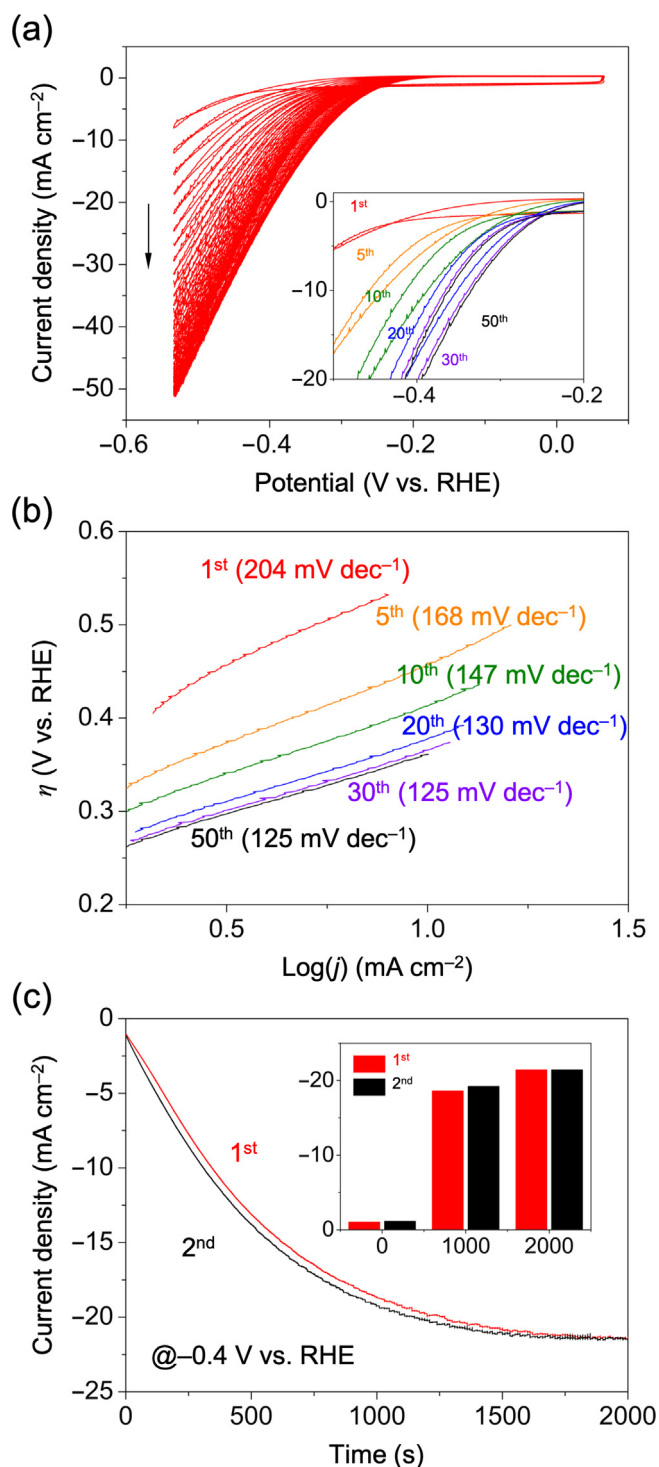
Fig. 2. (Color online) Electrochemical behaviour of $MoSi_2$. (a) CVs and (b) the corresponding Tafel plots of $MoSi_2$ in 1 mol L^{-1} KOH. (c) Chronoamperometric *i-t* curves of $MoSi_2$ at −0.4 V vs. RHE for different sequences in 1 mol L^{-1} KOH. Insets show the corresponding enlarged view and histogram of current densities in (a) and (c), respectively.

anomalous HER behavior of $MoSi_2$ in alkaline media is highly different from the common activation of other catalysts.

Next, we equipped a metal silicide library as model catalysts to identify the role of silicene subunit in alkaline HER. For WSi_2, whose crystal lattice is isomorphic to $MoSi_2$, a similar activation behavior was also observed in an alkaline media. Figs. 3a and S7 (online) show the crystal structure of WSi_2, consisting of alter-

nately stacked tungsten atom layers and silicene subunits. The activity of commercially available WSi_2 microparticles (Fig. S8 online) was enhanced several times after CV activation (Fig. 3d), and reached an equilibrium. Tafel slopes during this anomalous behavior were calculated in Fig. 3g. WSi_2 catalyst yields a far smaller Tafel slope of 168 mV dec^{-1} after activation, compared to its initial value (441 mV dec^{-1}). As expected, a high reversibility for this behavior was also observed (Fig. S9 online). $MoSi_2$ exhibits a much higher HER activity than that of WSi_2 and this indicates that Mo atom should outperform W atom as catalytically active site for HER. These results for WSi_2 again confirm the key role of silicene subunit edges in alkaline HER catalysis.

For $CrSi_2$ and $TaSi_2$ with a hexagonal C40 structure, their non-symmorphic $P6_222$ space group contains nonprimitive translations $\tau = c/3$ and $2c/3$ which interchange individual $CrSi_2$ or $TaSi_2$ layers, as shown in Fig. 3b and c. Each Cr/Ta and Si atom has six nearest planar neighbors within each hexagonal $CrSi_2$ or $TaSi_2$ layer, and four tetrahedral interplanar neighbors. Therefore, each Cr/Ta atom has four Si interplanar neighbors while each Si shares a pair of Cr/Ta and Si neighbors, forming a geometry with Cr/Ta atom arrays embedded in three-dimensional silicyne-wired networks. Detailed XRD and SEM data are shown in Figs. S10–13 (online). Further electrochemical tests for $CrSi_2$ and $TaSi_2$ do not reveal any anomalous activation behavior in alkaline media (Fig. 3e and f). Tafel slopes remain at an almost constant value after continues cycling (Fig. 3h and i). In addition, we evaluated the electrochemical behavior of FeSi, which features a simple-cubic structure with $P2_13$ space group. Fe and Si atom positions are represented as [1 1 1]-type displacements from those of a reference rocksalt structure (Fig. S14 online), where nearest-neighbor bonds include like-numbered Fe(n)–Si(n) pairs located either within central cell (n = 1) or across cell-boundary edges (n = 2–4). Cubic FeSi also does not exhibit an anomalous activation behavior (Fig. S15 online). These results suggest that only those metal silicides containing silicene subunits show anomalous HER catalysis.

3.3. Surface evolution

To probe the surface evolution of $MoSi_2$, both the catalysts before and after activation were analyzed by X-ray photoelectron spectroscopy (XPS). As shown in Fig. 4a, the Mo 3*d* spectra of two samples both display one peak at ~228 eV, attributed to Mo^0 in the form of $MoSi_2$ [24]. Two Mo oxide species, including MoO_2 and MoO_3, were also detected. Although the Mo 3*d* XPS signal weakens after activation, the shape remains basically unchanged. One shoulder peak at ~100 eV in both Si 2*p* spectra (Fig. 4b) is characteristic of Mo–Si bonds in $MoSi_2$ [29], whereas a pronounced peak attributed to silicon oxide at ~102 or 103 eV was observed for two $MoSi_2$. After activation, the main Si 2*p* peak sharpens and shifts to lower binding energy, while its shoulder weakens. This indicates that the Mo–Si bond strength decreases, and the Si atoms appear partially oxidized on the very surface of $MoSi_2$. High-resolution transmission electron microscopy (HRTEM) image of $MoSi_2$ after alkaline HER along the [1–10] zone axis is presented in Fig. 4c. The image further demonstrates the presence of a thin amorphous shell on the $MoSi_2$ surface. Two fast Fourier transform (FFT) patterns also confirm the surface amorphization (Fig. 4d and e). The oxidation state of Si in pristine $MoSi_2$ is indeed zero, and the occurrence of partially oxidized Si and amorphous shell cannot be attributed to the cathodic HER, which takes place under reduction potentials.

Si element has an amphoteric nature, but similar activation behavior does not happen in acid media (Fig. S16 online). Therefore, it can occur due to the OH$^-$ ions from KOH aqueous electrolyte and water dissociation during alkaline HER process. The surface Si atoms would be partially oxidized by the adsorption of
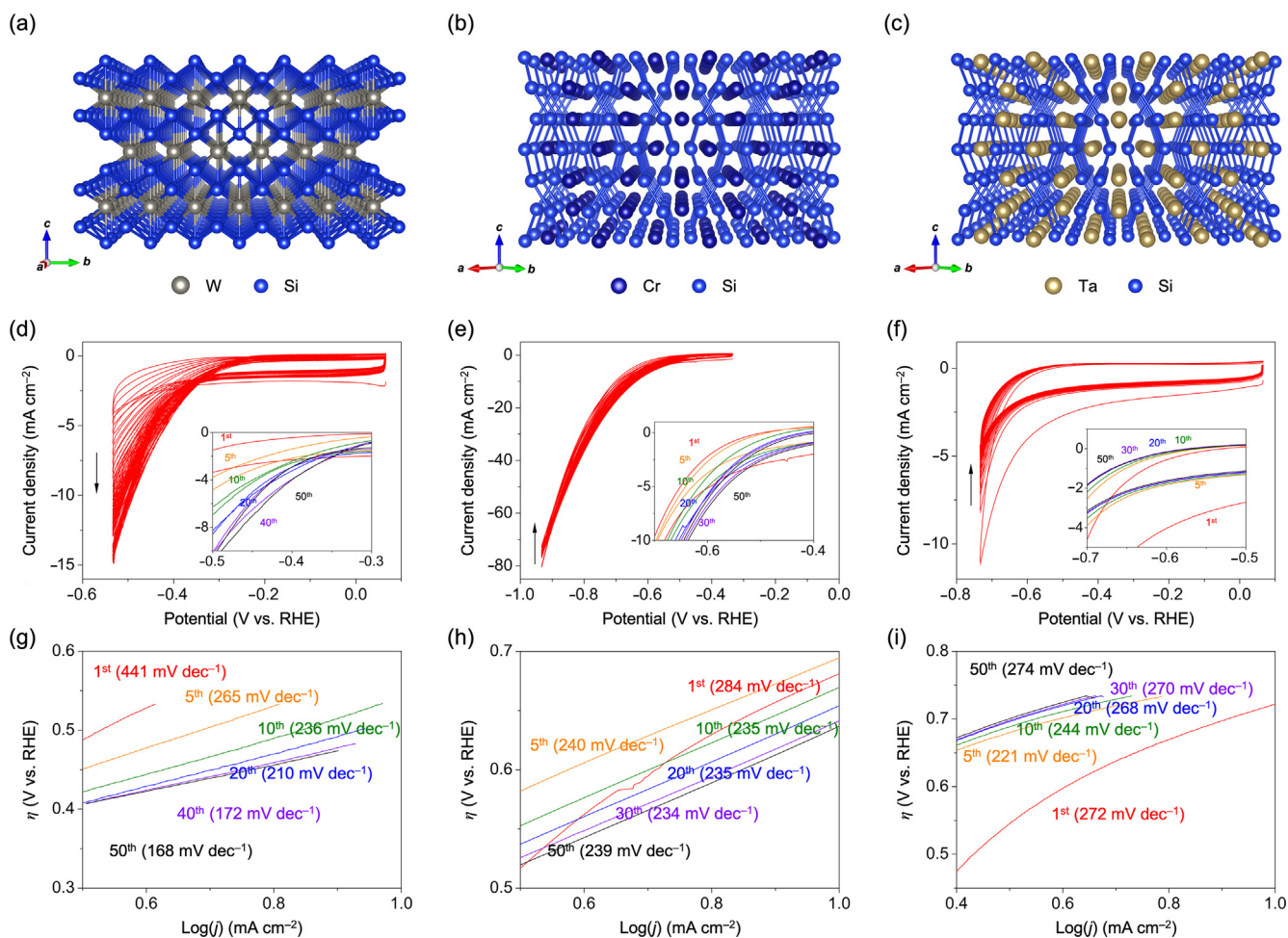
Fig. 3. (Color online) Electrochemical behaviour of other silicides. (a–c) Crystal structure of WSi_2, $CrSi_2$, and $TaSi_2$. (d–f) CVs and (g–i) the corresponding Tafel plots of WSi_2, $CrSi_2$, and $TaSi_2$ in 1 mol L^{-1} KOH. Insets show the corresponding enlarged views in (d–f).

OH^- ions, forming kinetically favored Si–OH bonds, and in general, Si oxidation mainly involves Si–Si bond cleavage and Si reacting with water to yield hydrogen and silicate (Fig. S17 online) [30,31]. Such an oxidation process is clearly supported by the inductively coupled plasma-optical emission spectrometry (ICP-OES) detection of Si signal in an electrolyte after CV activation (Table S2 online).

Once the electrode is immersed into KOH electrolyte, Si–OH bonds would be formed on the $MoSi_2$ surface. However, when HER initiates, the surfaces of cathode and anode become negatively and positively charged respectively, leading to the localization of OH^- ions of alkaline electrolyte on the anode, rather than cathode [32,33]. Thus, the electric field determined by the electrical double layer at the anode–electrolyte interface inevitably weakens the strength of the Si–OH bond, and forces negatively charged OH^- to be detached from the $MoSi_2$ surface. On the other hand, surface Mo of the catalyst triggers the adsorption and dissociation of water molecules, leading to continuous OH^- production. Dissociated OH^- ions can readily bind to the neighboring Si, forming new Si–OH bonds on $MoSi_2$ (Fig. S18 online). These two competing effects, which influence each other throughout the HER process, control the HER activity of $MoSi_2$ catalyst, and jointly cause the anomalous electrochemical behavior.

3.4. Theoretical computations

To provide atomic-level understanding, we used density functional theory (DFT) calculations to determine the detailed energy profiles of HER pathways on the Mo atoms surrounded by Si edge atoms in silicenes with different surface state, containing either OH^- terminations or edge vacancies (Figs. 5a, b, and S19 online). Although we found that the surface of $MoSi_2$ after alkaline HER catalysis becomes an amorphous phase with long-range disorder from the TEM images, both the crystalline and amorphous surfaces of $MoSi_2$ should have a similar atomic-scale structure with the same short-range order and coordination environment. Therefore, we chose the periodic model as a compromise. As revealed experimentally, cathodic HER on $MoSi_2$ proceeds according to Volmer–Heyrovsky mechanism, which mainly involves proton adsorption and reduction on the active center, followed by electrochemical dihydrogen desorption [34]. Clearly, the reaction energy of proton adsorption on Mo exhibits a strong dependence on the coverage of adsorbed OH^- on silicene subunit edges (Fig. 5b). When the number of adsorbed OH^- is decreased from four to one, the reaction energy of $H_2O^* + H_2O \rightarrow OH^* + H^* + H_2O$ is greatly decreased from 0.58 to 0.15 eV (where "*" indicates adsorbed species). The calculations demonstrate that a $MoSi_2$ surface with fewer Si–OH bonds shows a higher HER activity. As mentioned above, the initiation of cathodic HER leads to the cleavage of Si–OH bonds, but the dissociation of water molecules induces the formation of new Si–OH bonds. These two competing effects fluctuate during HER catalysis at different rates, denoted by v_1 and v_2, respectively. As depicted in Figs. S18 and S20 (online), we start with an almost fully OH^--covered catalyst surface and a poor catalytic efficiency, therefore, $v_1 > v_2$. Then, the initially existing Si–OH bonds continually decrease in number, and v_2 becomes faster, forming more active
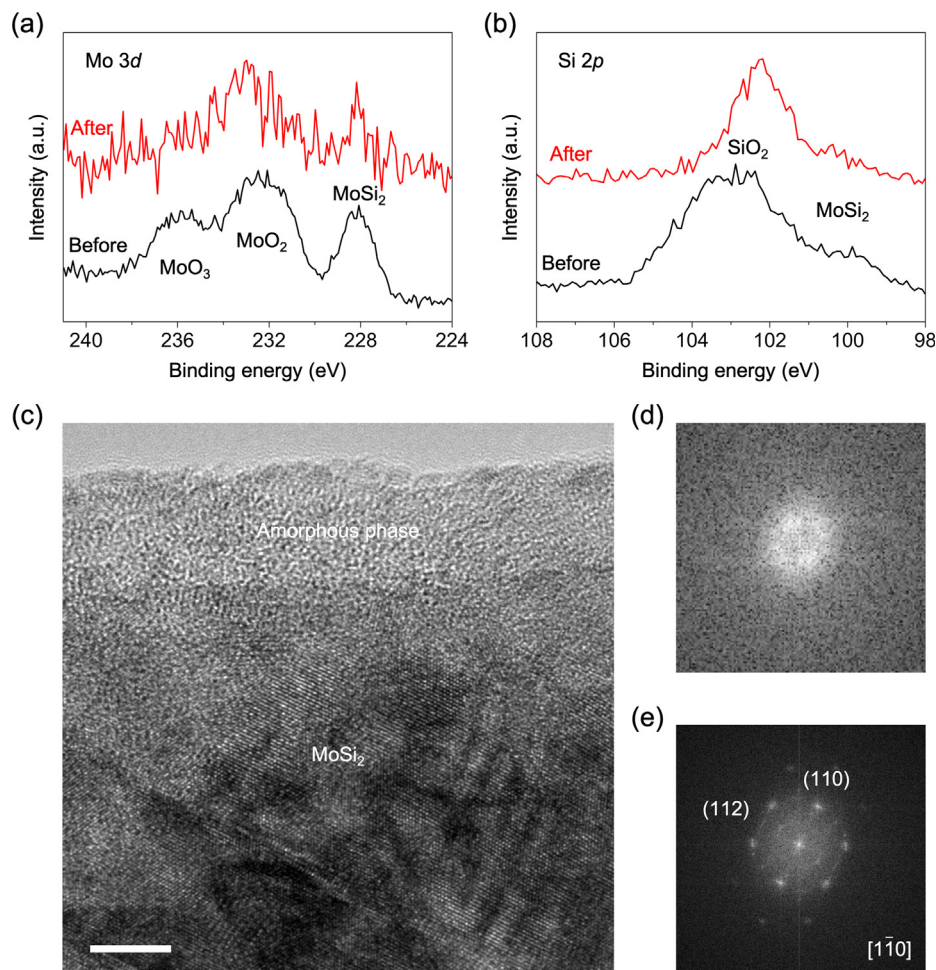
Fig. 4. (Color online) Surface evolution of MoSi$_2$. (a) Mo 3d and (b) Si 2p XPS spectra of MoSi$_2$ before and after CV activation in 1 mol L^{-1} KOH. (c) HRTEM image of MoSi$_2$ after activation along the [1–10] zone axis, with a low-contrast thin layer indicating the silicon oxide shell. (d) Fourier transform images of the amorphous shell and (e) MoSi$_2$ core. Scale bar is 5 nm.

Mo centers and new Si–OH bonds. This fluctuation finally reaches equilibrium ($v_1 = v_2$), in which the amounts of formed and broken Si–OH bonds per unit time are the same, and the catalytic activity of Mo reaches the maximum (Figs. 2 and S20 online). Once the cathodic voltage is withdrawn, both v_1 and v_2 return to zero, and the edges of silicene subunit become fully covered with OH$^-$ again. Such a recurrence causes the inactivation of MoSi$_2$, and satisfactorily explains the anomalous activation with a high reversibility (Fig. 2c).

Some edge Si vacancies ineluctably appear during silicene subunit oxidation, and these formed nonmetal defects change the local environment of Mo [35,36]. As shown in Fig. 5b, more Si vacancies make Mo center more active for catalyzing two-electron reduction of two protons to yield dihydrogen, as the overall reaction energies are greatly lessened. The same conclusion can be further supported by analyzing the projected density of states (PDOS) onto Mo 4d states for MoSi$_2$ surfaces with different densities of Si vacancy (Fig. 5c). The PDOS across the Fermi level increases with increasing vacancy density, and the positions of Mo 4d and Si 2p-band centers also shift up while the energy difference between them decreases from 1.21 to 1.00 eV (Table S3 online). These results indicate that the formation of Si vacancies on silicene subunit edges weakens the covalent character of Mo–Si bonds, and enhances the metallicity and catalytic activity of Mo. Thus, the slight enhancement in current density between the first and second chronoamperometric curve can be well interpreted (Fig. 2c). In close comparison with

the stable CV curves of MoSi$_2$ recorded in acid and alkaline media, we found that MoSi$_2$ catalyst exhibits a higher activity for alkaline HER (Fig. S21 online). Although the Si–OH bonds on silicene subunit edges restrain the proton adsorption and reduction on the local Mo sites, the formation of new Si–OH bonds during HER catalysis accelerates the kinetics of rate-limiting water dissociation, and in turn contributes to the activity enhancement of Mo (Fig. S22 online). We can expect a better activity for alkaline HER through coupling catalyst with silicene or other Si allotropes to more efficiently dissociate the water molecules.

4. Conclusions

In summary, we present an anomalous HER behavior of MoSi$_2$ catalyst comprising silicene subunits in alkaline media. One order of magnitude enhancement of activity is achieved after a continuous operation, yielding an increased current density from 1.1 to 21.5 mA cm^{-2} at an overpotential of 0.4 V. This activation behavior also exhibits a high reversibility, in which voltage withdrawal leads to catalyst inactivation but another operation causes reactivation. Isomorphic WSi$_2$ behaves almost the same as MoSi$_2$, whereas other metal silicides with silicyne subunits, including CrSi$_2$ and TaSi$_2$, do not exhibit any anomalous behavior. A thin amorphous shell of MoSi$_2$ is observed after the reaction, within which the Si remains partially oxidized and the oxidation state of Mo is basically unchanged. We find that the coverage of adsorbed
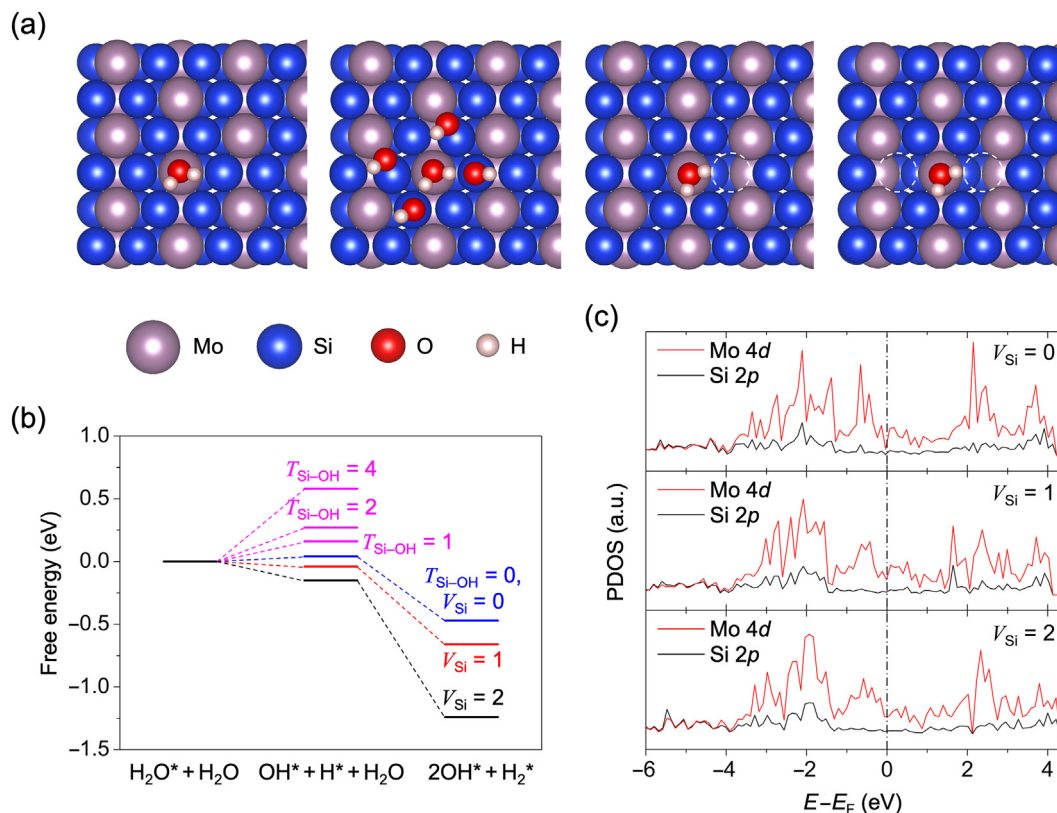
Fig. 5. (Color online) Density functional theory calculations of hydrogen evolution on $MoSi_2$. (a) Optimized geometry of pristine $MoSi_2$ (1 1 0) surface with adsorbed H_2O and other $MoSi_2$ (110) surfaces with adsorbed H_2O and OH groups/Si vacancies. (b) Free energy versus the reaction coordinate of alkaline HER for different $MoSi_2$ surfaces. (c) Calculated projected density of states (PDOS) plots of Mo $4d$ and Si $2p$ orbitals for pristine $MoSi_2$ and other $MoSi_2$ surfaces with Si vacancies.

hydroxide ions on the edges of silicene subunits in $MoSi_2$ and the Si vacancy formation both alter the HER kinetics of the local Mo active sites. Such an anomalous behavior can be explained as the synergy between the hydrogen evolution on Mo and partial oxidation of silicene subunits. This work demonstrates that the role of nonmetal varies dramatically with the electronic and crystallographic structures if silicides and that silicene structural unit may serve as a promoter for boosting HER in alkaline media.

Conflict of interest

The authors declare that they have no conflict of interest.

Acknowledgments

Author contributions

L.M. and Z.Z. proposed and designed the research. Z.Z., J.H., and Z.L. performed the materials synthesis and electrochemical analyses. Z.Z., J.H., and Z.L. conducted the materials characterization. Y. L. and L.V.M. designed and conducted the DFT computations. Z.Z., and Y.L. co-wrote the paper. All authors discussed the results and commented on the manuscript.

Appendix A. Supplementary data

Supplementary data to this article can be found online at https://doi.org/10.1016/j.scib.2019.04.005.

References

[1] Lin L, Zhou W, Gao R, et al. Low-temperature hydrogen production from water and methanol using Pt/α-MoC catalysts. Nature 2017;544:80–3.

[2] Jaramillo TF, Jorgensen KP, Bonde J, et al. Identification of active edge sites for electrochemical H_2 evolution from MoS_2 nanocatalysts. Science 2007;317:100–2.

[3] Li H, Tsai C, Koh AL, et al. Activating and optimizing MoS_2 basal planes for hydrogen evolution through the formation of strained sulphur vacancies. Nat Mater 2016;15:48–53.

[4] Tran PD, Tran TV, Orio M, et al. Coordination polymer structure and revisited hydrogen evolution catalytic mechanism for amorphous molybdenum sulfide. Nat Mater 2016;15:640–6.

[5] Kibsgaard J, Chen Z, Reinecke N, et al. Engineering the surface structure of MoS_2 to preferentially expose active edge sites for electrocatalysis. Nat Mater 2012;11:963–9.

[6] Wang J, Yan M, Zhao K, et al. Field effect enhanced hydrogen evolution reaction of MoS_2 nanosheets. Adv Mater 2017;29:1604464.

[7] Wan C, Regmi YN, Leonard BM. Multiple phases of molybdenum carbide as electrocatalysts for the hydrogen evolution reaction. Angew Chem Int Ed 2014;53:6407–10.

[8] Jin Y, Wang H, Li J, et al. Porous MoO_2 nanosheets as non-noble bifunctional electrocatalysts for overall water splitting. Adv Mater 2016;28:3785–90.

[9] Jin Y, Wang H, Li J, et al. Porous molybdenum phosphide nano-octahedrons derived from confined phosphorization in UIO-66 for efficient hydrogen evolution. Angew Chem Int Ed 2016;55:12854–8.

[10] Chen Y, Yu G, Chen W, et al. Highly active, nonprecious electrocatalyst comprising borophene subunits for the hydrogen evolution reaction. J Am Chem Soc 2017;139:12370–3.

[11] Vrubel H, Hu X. Molybdenum boride and carbide catalyze hydrogen evolution in both acidic and basic solutions. Angew Chem Int Ed 2012;51:12703–6.
[12] Van der Zande AM, Huang PY, Chenet DA, et al. Grains and grain boundaries in highly crystalline monolayer molybdenum disulphide. Nat Mater 2013;12:554–61.
[13] Koh MJ, Nguyen TT, Lam JK, et al. Molybdenum chloride catalysts for Z-selective olefin metathesis reactions. Nature 2017;542:80–5.
[14] Park H, Encinas A, Scheifers JP, et al. Boron-dependency of molybdenum boride electrocatalysts for the hydrogen evolution reaction. Angew Chem Int Ed 2017;56:5575–8.
[15] Xu C, Wang L, Liu Z, et al. Large-area high-quality 2D ultrathin Mo_2C superconducting crystals. Nat Mater 2015;14:1135–41.
[16] Yin Y, Han J, Zhang Y, et al. Contributions of phase, sulfur vacancies, and edges to the hydrogen evolution reaction catalytic activity of porous molybdenum disulfide nanosheets. J Am Chem Soc 2016;138:7965–72.
[17] Cui J, Wong YL, Zeller M, et al. Pd uptake and H_2S sensing by an amphoteric metal–organic framework with a soft core and rigid side arms. Angew Chem Int Ed 2014;53:14438–42.
[18] Jaramillo TF, Bonde J, Zhang J, et al. Hydrogen evolution on supported incomplete cubane-type $[Mo_3S_4]^{4+}$ electrocatalysts. J Phys Chem C 2008;112:17492–8.
[19] Kibsgaard J, Jaramillo TF, Besenbacher F. Building an appropriate active-site motif into a hydrogen-evolution catalyst with thiomolybdate $[Mo_3S_{13}]^{2-}$ clusters. Nat Chem 2014;6:248–53.
[20] Zhang XY, Sprengel W, Staab TEM, et al. Formation of thermal vacancies on the Si sublattice of the intermetallic compound $MoSi_2$. Phys Rev Lett 2004;92:155502.
[21] VandeVondele J, Krack M, Mohamed F, et al. Quickstep: fast and accurate density functional calculations using a mixed Gaussian and plane waves approach. Comput Phys Commun 2005;167:103–28.
[22] Perdew JP. Density-functional approximation for the correlation energy of the inhomogeneous electron gas. Phys Rev B 1986;33:8822.
[23] Perdew JP, Burke K, Ernzerhof M. Generalized gradient approximation made simple. Phys Rev Lett 1996;77:3865–8.
[24] Grimmea S, Antony J, Ehrlich S, et al. A consistent and accurate *ab initio* parametrization of density functional dispersion correction (DFT-D) for the 94 elements H-Pu. J Chem Phys 2010;132:154104.
[25] Goedecker S, Teter M, Hutter J. Separable dual-space Gaussian pseudopotentials. Phys Rev B 1996;54:1703.
[26] Barbieri L, Bondioli F, Lancellotti I, et al. The anorthite–diopside system: structural and devitrification study. Part II: crystallinity analysis by the Rietveld–RIR Method. J Am Ceram Soc 2005;88:3131–6.
[27] Ma R, Zhou Y, Chen Y, et al. Ultrafine molybdenum carbide nanoparticles composited with carbon as a highly active hydrogen-evolution electrocatalyst. Angew Chem Int Ed 2015;54:14723–7.
[28] Lukowski MA, Daniel AS, Meng F, et al. Enhanced hydrogen evolution catalysis from chemically exfoliated metallic MoS_2 nanosheets. J Am Chem Soc 2013;135:10274–7.
[29] Shaw L, Abbaschian R. Chemical states of the molybdenum disilicide ($MoSi_2$) surface. J Mater Sci 1995;30:5272–80.
[30] Luo Z, Jiang Y, Myers BD, et al. Atomic gold–enabled three-dimensional lithography for silicon mesostructures. Science 2015;348:1451–5.
[31] Huang Z, Geyer N, Werner P, et al. Metal-assisted chemical etching of silicon: a review. Adv Mater 2011;23:285–308.
[32] Danilovic N, Subbaraman R, Strmcnik D, et al. Enhancing the alkaline hydrogen evolution reaction activity through the bifunctionality of $Ni(OH)_2$/metal catalysts. Angew Chem Int Ed 2012;51:12495–8.
[33] Ledezma-Yanez I, Wallace W, Sebastián-Pascual P, et al. Interfacial water reorganization as a pH-dependent descriptor of the hydrogen evolution rate on platinum electrodes. Nat Energy 2017;2:17031.
[34] Tian J, Liu Q, Asiri AM, et al. Self-supported nanoporous cobalt phosphide nanowire arrays: an efficient 3D hydrogen-evolving cathode over the wide range of pH 0–14. J Am Chem Soc 2014;136:7587–90.
[35] Vandré S, Kalka T, Preinesberger C, et al. Flatband conditions observed for lanthanide-silicide monolayers on *n*-type Si(111). Phys Rev Lett 1999;82:1927–30.
[36] Liu G, Young KL, Liao X, et al. Anisotropic nanoparticles as shape-directing catalysts for the chemical etching of silicon. J Am Chem Soc 2013;135:12196–9.

Zechao Zhuang received his Master of Engineering degree from Fujian Normal University in 2015. He is currently a Ph. D. candidate under supervision of Prof. Liang Zhou and Prof. Liqiang Mai in Wuhan University of Technology. His research interests mainly focus on electron-structure-oriented design and synthesis of advance electrocatalysts for water splitting, fuel cell, and carbon dioxide reduction.

Lyudmila V. Moskaleva is an Associate Professor at the Department of Chemistry, the University of the Free State, South Africa. She received her Ph.D. degree from Emory University, USA, in 2001 and carried out her postdoctoral research at Emory University in 2001 and Technical University of Munich, Germany, as a Humboldt Research Fellow in 2002–2006. Subsequently, she was a senior scientist at the Institute of Applied and Physical Chemistry at the University of Bremen, Germany, in 2009–2018. Her research interests include catalysis, electrocatalysis, theoretical chemistry, and surface chemistry.

Liqiang Mai is Chang Jiang Scholar Chair Professor of Materials Science and Engineering at Wuhan University of Technology (WUT), Dean for School of Materials Science and Engineering at WUT, and Fellow of the Royal Society of Chemistry. He received his Ph.D. degree from WUT in 2004 and carried out his postdoctoral research in Prof. Zhonglin Wang's group at Georgia Institute of Technology in 2006–2007. He worked as an advanced research scholar in Prof. Charles M. Lieber's group at Harvard University in 2008–2011 and Prof. Peidong Yang's group at University of California, Berkeley in 2017. His current research interests focus on new nanomaterials for electrochemical energy storage and micro/nano energy devices.